Seismotectonic Interpretation of the 2015 Sandpoint, Idaho, Earthquake Sequence

Daisuke Kobayashi
Kenneth F. Sprenke
Michael C. Stickney
William M. Phillips

Idaho Geological Survey
University of Idaho
875 Perimeter Drive MS 3014
Moscow, Idaho 83844-3014
www.IdahoGeology.org

Staff Report 16-1
August 2016

Seismotectonic Interpretation of the 2015 Sandpoint, Idaho, Earthquake Sequence

Daisuke Kobayashi[1]
Kenneth F. Sprenke[1]
Michael C. Stickney[2]
William M. Phillips[3]

Staff Reports present timely information for public distribution. This publication may not conform to the Agency's standards.

Idaho Geological Survey
University of Idaho
875 Perimeter Drive MS 3014
Moscow, Idaho 83844-3014
www.IdahoGeology.org

Staff Report 16-1
August 2016

[1]Department of Geological Sciences, University of Idaho, Moscow, Idaho 83844-3022
[2]Montana Bureau of Mines and Geology, Butte, Montana 59701-8997
[3]Idaho Geological Survey, University of Idaho, Moscow, Idaho 83844-3014

Contents

ABSTRACT....1

INTRODUCTION....1

REGIONAL TECTONIC SETTING AND SEISMICITY....2

THE 24 APRIL 2015 SANDPOINT EARTHQUAKE SEQUENCE....9

FAULT PLANE SOLUTIONS....13

TECTONIC IMPLICATIONS....17

CONCLUSIONS....20

ACKNOWLEDGMENTS....22

REFERENCES....23

APPENDIX....29

Figures

Figure 1. Regional tectonic setting and seismicity....2

Figure 2. Tectonic map of eastern Washington, northern Idaho, and northwestern Montana showing major faults....3

Figure 3. Simplified early interpretations of the relation between the Hope and Purcell Trench faults....6

Figure 4. Timelines of instrumentally determined earthquakes in the Lake Pend Oreille - area....8

Figure 5. Spatial distribution of epicenters from 1982 through 2014 and in 2015....9

Figure 6. Epicenters of the Sandpoint earthquakes by this study and the USGS (U.S. Geological Survey, 2015a, b), and aftershocks during the first three months after the Sandpoint events....11

Figure 7. Seismograms of the second event of the Sandpoint sequence recorded at 9 selected stations 12

Figure 8. Recorded (a) peak acceleration, (b) peak velocity, and (c) instrumental intensity of the first event of the Sandpoint sequence, and (d-f) those of the second event.....14

Figure 9. Fault plane solutions for the (a) first, (b) second, and (c) third events of the Sandpoint earthquakes 16

Figure 10. Moment tensor solutions for the (a) first and (b) second events of the Sandpoint earthquakes by the USGS (U.S. Geological Survey, 2015a, b).....17

Figure 11. (a) Epicenters and focal mechanism solutions of the Sandpoint sequence by this study and the U.S. Geological Survey (2015a, b), and fault distribution in the epicentral area 18

Figure 12. GPS velocity field of the northwestern U.S. (McCaffrey and others, 2007, 2013) showing a clockwise crustal rotation relative to the North American plate.....19

Figure 13. T-axes from fault plane solutions of the Sandpoint earthquakes and the adjacent events (see Figure 12 for earthquake location), and from the best-fit and alternate allowable models of the 2001 Spokane sequence (Wicks and others, 2013).....20

Figure 14. Dilatational strain rate (dilatation positive) calculated from GPS horizontal velocities 22

Tables

Table 1. Origin details of the Sandpoint earthquakes sequence on April 24th, 2015.....13

Table 2. Fault plane solution of the Sandpoint earthquakes 14

Table 3. Source parameters of the Sandpoint earthqakes determined by the USGS 17

ABSTRACT

A sequence of three earthquakes, M4.1, M4.2, and M3.5, occurred in the vicinity of Sandpoint, Idaho, on April 24th 2015. These events were followed by an elevated rate of seismicity. The mainshocks occurred southeast of the intersection between the southwest dipping Hope fault and east-southeast dipping Purcell Trench fault within the Lewis Clark Fault Zone (LCFZ), and weakly shook the area in eastern Washington, northern Idaho, and northwestern Montana. We present fault plane solutions of the three Sandpoint events from P-wave first motion data recorded at stations operated by the Montana Bureau of Mines and Geology, University of Washington, U.S. Geological Survey, Canadian Geological Survey, Idaho National Labs, University of Utah, and NIOSH Spokane Mining Research Division, and compare them with moment tensor solutions by the U.S. Geological Survey (USGS). All of our fault plane solutions show a reverse sense of oblique slip on a northeast striking southeast dipping nodal plane, which is inconsistent with focal mechanisms of the historical events in the central and eastern parts of the LCFZ, which indicates northeast-southwest extension. The reverse mechanisms are likely to represent a reactivation of the east-southeast dipping Purcell Trench fault. A recent GPS velocity field and strain analysis indicate possible contraction in the epicentral area. The Sandpoint earthquakes, along with the adjacent reverse-faulting events, constrain the western extent of the northeast-southwest extension of the LCFZ.

INTRODUCTION

A sequence of three M3-4 earthquakes occurred around Lake Pend Oreille southeast of Sandpoint, Idaho, on April 24th 2015 (Figure 1). Because they were widely felt in much of northeastern Washington, northern Idaho, and northwestern Montana, a region of relatively low seismicity, these events were reported in the press across the region. These earthquakes occurred where the two major faults in the area, the Hope fault and Purcell Trench fault, converge (Figures 1 and 2). The southwest dipping Hope fault is in the western part of the Lewis Clark Fault Zone, a zone of complex, steeply dipping faults that extends to western Montana (Foster and others, 2007, and references therein). The Hope fault is truncated against an east-southeast dipping segment of the Purcell Trench fault in the epicentral area (Figures 1 and 2). The Purcell Trench fault extends from the Lake Coeur d'Alene area to southeastern British Columbia (Clark, 1973), marking the eastern boundary of the Priest River metamorphic core complex (Figure 2) (e.g., Harms and Price, 1992; Doughty and Price, 1999, 2000). We found fault plane solutions of the three Sandpoint earthquakes inconsistent with a northeast-southwest extension indicated by historical seismicity in the Lewis Clark Fault Zone (Stickney and Bartholomew, 1987; Stickney, 2015). In this report, we present the fault plane solutions and a seismotectonic analysis to explain these unusual mechanisms.

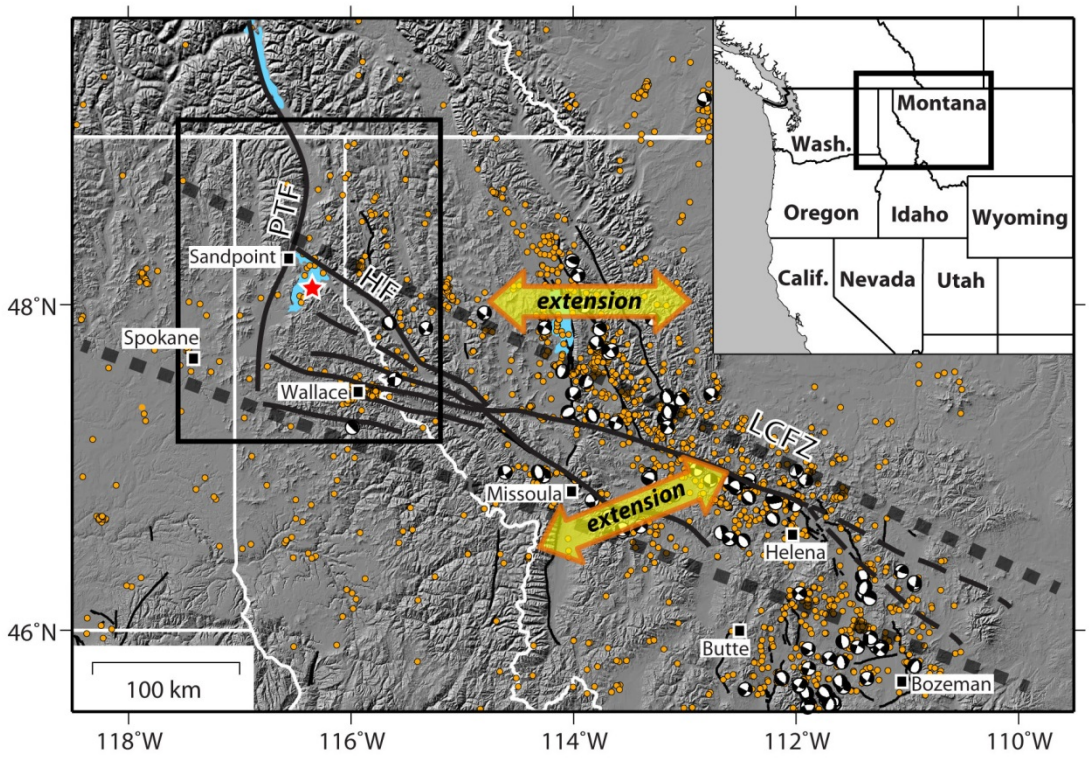

Figure 1**.** Regional tectonic setting and seismicity. Red star indicates the epicentral area of the 24 April 2015 Sandpoint sequence. Thick dark gray dotted lines bracket the Lewis Clark Fault Zone (LCFZ). Thick black lines represent the Purcell Trench fault (PFT) and the major faults in the LCFZ including the Hope fault (HF) (modified from Foster and others, 2007). Thin black lines represent Quaternary faults. Orange dots represent earthquake epicenters (M>1.5; 2000-2013), and focal mechanisms are for M>2.5 events (1982-2014) (M.C. Stickney, unpublished data, 2015). Seismicity indicates east-west extension to the north of the LCFZ and northeast-southwest extension within and south of the central and eastern LCFZ (yellow arrows; Stickney, 2015). Box in main map outlines area of Figure 2. White lines indicate national and state boundaries. Elevation data from Gesch (2007) and Gesch and others (2002). Inset shows location of the map area.

REGIONAL TECTONIC SETTING AND SEISMICITY

The Sandpoint earthquake sequence occurred approximately 23 km (14 mi) southeast of Sandpoint, Idaho, near Lake Pend Oreille. The epicentral area is in the western part of the Lewis Clark Fault Zone, where major faults, the Hope, Purcell Trench, and Newport faults interact (Figures 1 and 2).

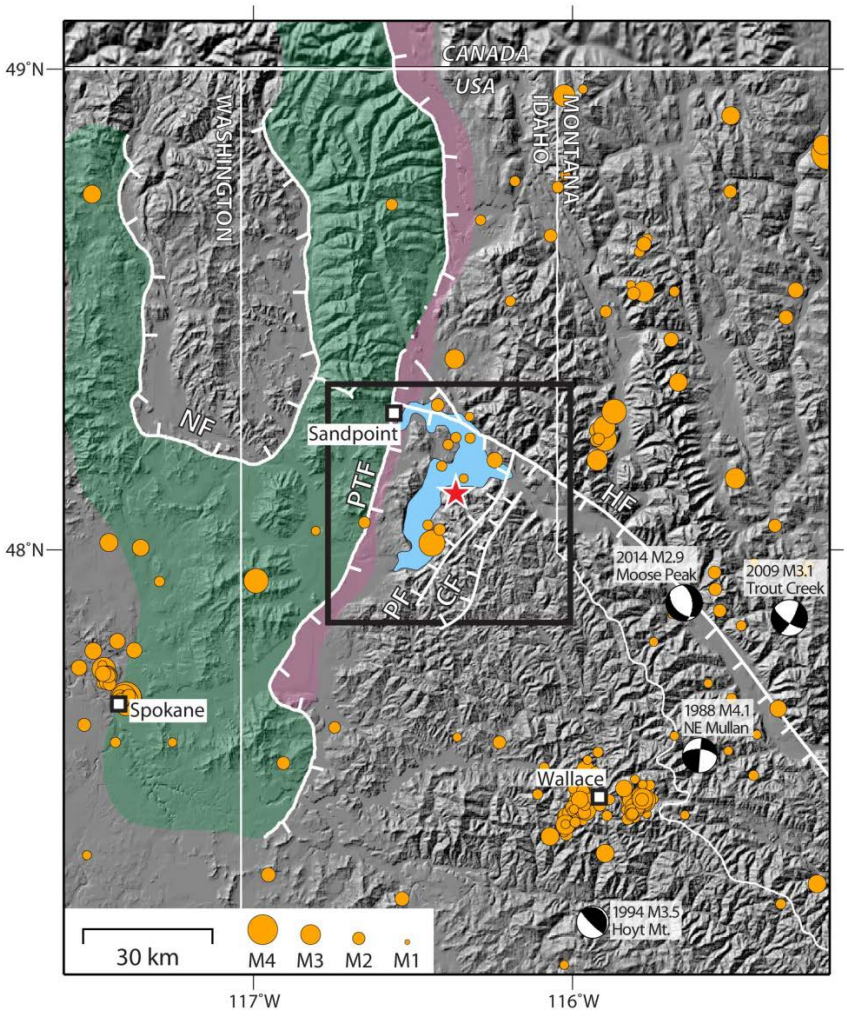

Figure 2**.** Tectonic map of eastern Washington, northern Idaho, and northwestern Montana showing major faults (modified from Doughty and Price 1999, 2000; Foster and others, 2007). See Figure 1 for location of the map area. Hachures on a fault trace indicate the down-thrown side of a normal fault. NF, Newport fault; PTF, Purcell Trench fault; HF, Hope fault; PF, Packsaddle fault; CF, Cascade fault. Dotted line represents an unfaulted segment of the Purcell Trench Fault (Doughty and Price, 1999, 2000). Red star indicates the epicentral area. Orange dots represent earthquake epicenters (M>1.5; 2000-2013; scaled by magnitude), and focal mechanisms are for major earthquakes around the epicenters (Sprenke et al., 1991, 1994; M.C. Stickney, personal communication, 2013). Green shaded area represents the Priest River metamorphic core complex, and pink shaded area represents the Purcell trench. Light blue area represents Lake Pend Oreille. Box outlines area for earthquake timelines in Figure 4.

The epicenters of the Sandpoint earthquakes are in the western part of the Lewis Clark Fault Zone (LCFZ), a ~800 km (500 mi) long, 80-100 km (50-62 mi) wide, east-southeast trending structural discontinuity extending from central Washington to western Montana (Figure 1;

Harrison and others, 1974; Stickney and Bartholomew, 1987). The fault zone is characterized by a complex series of steeply dipping, northwest striking strike-slip, oblique-slip, and dip-slip faults due to multiple reactivation episodes (Harrison and others, 1974; Foster and others, 2007). The fault zone formed in early Mesoproterozoic (1.5 to 1.4 Ga) in association with rifting and the Belt basin formation (Smith, 1965; Harrison and others, 1974; Reynolds, l979; Winston, 1986; Wallace and others, 1990; Sears and Hendrix, 2004). During Cretaceous to Paleogene, the LCFZ accommodated sinistral transpression, crustal shortening in a left-lateral sense, as a result of thrusting and batholith intrusions (Hyndman and others, 1988; Sears and others, 2000; Sears and Hendrix, 2004). In response to crustal collapse of the Cretaceous-Paleocene orogenic wedge (Coney, 1987; Harry and others, 1993; Livaccari, 1991; Sonder and others, 1987; Wernicke and others, 1987), the Eocene extension took place, reactivating the LCFZ as a dextral shear zone to accommodate differential extension (Reynolds, 1979; Doughty and Sheriff, 1992; Foster and Fanning, 1997; Sears and Fritz, l998; Lewis and others, 2005).

Active seismicity has been observed within the LCFZ and the adjacent areas (Figure 1). The eastern LCFZ is associated with recurrent seismicity including multiple M~6 events resulted from normal slip near Helena, Montana (Freidline and others, 1976; Stickney, 1978; Stickney and Bartholomew, 1987). In the central and eastern LCFZ and the area south of the LCFZ, both major and small events indicate a northeast-southwest extension (Figure 1) (Stickney and Bartholomew, 1987; Stickney, 2015). To the north of the LCFZ, predominant directions of principal stress have been unclear (Sbar and others, 1972; Stevenson, 1976; Stickney, 1980; Qamar and others, 1982) until a recent seismotectonic analysis by Stickney (2015) suggested an east-west extension (Figure 1). In the western part of the LCFZ, diffuse seismicity, including events as large as M~5, has been recorded. M~5 events occurred in 1918 in Rathdrum, Idaho, and in 1942 in Sandpoint (Sprenke and Breckenridge, 1992). Figure 2 shows instrumentally recorded earthquakes since 2000 and focal mechanisms of the major events in eastern Washington, northern Idaho, and northwestern Montana. The August 1, 1988 tectonic earthquake (M4.1) northeast of Mullan resulted from dextral slip, possibly along the west-northwest striking Thompson Pass Fault (Sprenke and others, 1991). Another notable earthquake in the area is the 1994 M3.5 Hoyt Mountain event followed by a M2.9 aftershock. Both mainshock and aftershock indicate a reverse reactivation of a steeply dipping (~75°) northwest-southeast striking relict normal fault (Sprenke and others, 1994). The 2009 M3.1 Trout Creek and the 2014 M2.9 Moose Peak earthquakes were located near Trout Creek, Montana, about 90 km (56 mi) southeast of Sandpoint. Relatively concentrated seismicity in the Wallace area is mostly from mining-related rockbursts (Figure 1) (Stickney and Bartholomew, 1987; Sprenke and others, 1991). In the Spokane area, there is another concentrated seismicity, which represents a five month long swarm of small earthquakes that occurred in 2001 (Wicks and others, 2013).

The main fault in the LCFZ is splayed in northwestern Montana toward the western end of the fault zone (Figure 1). The northernmost of these splays is the southwest dipping Hope fault, which terminates against the Purcell Trench fault in the epicentral area (Figure 2). The Hope fault formed in Proterozoic (Harrison and others, 1972) and reactivated as a dip-slip fault in early Eocene (Fillipone and Yin, 1994; Fillipone and others, 1995). A dextral normal sense of motion is indicated as the latest movement along the Hope fault (e.g., Harrison and Jobin, 1963),

which is consistent with the fault plane solution of events that occurred near the structure (i.e., the 2000 Trout Creek and 2014 Moose Peak events; Figure 2).

The Purcell Trench fault is an east-southeast dipping listric detachment fault that extends from Coeur d'Alene Lake to southeastern British Columbia (Figures 1 and 2) (Reynolds 1980; Rehrig and others, 1987; Doughty and Price, 1999, 2000). Along its trace, the Purcell Trench fault forms a half-graben, the Purcell trench, which is a 5-7 km (3-4.3 mi) wide topographic depression (Figure 2) locally filled with Tertiary sediments and covered by glacial deposits. The Hope fault terminates against the Purcell Trench fault to the immediate north of Sandpoint (Figure 2). The Purcell Trench fault formed to accommodate the Eocene extension and became a detachment fault verging to the east that unroofed the Priest River metamorphic core complex on its western side (Figure 2) (Rehrig and others, 1987; Harms and Price, 1992; Doughty and Price, 1999, 2000).

The presence and nature of the Purcell Trench fault and its relation to the Hope fault were unclear for decades mainly because: (1) the fault was mostly covered by glacial deposits in the Purcell trench; and (2) metamorphic core complexes (MCC), one of which forms the foot-wall block of the Purcell Trench fault, were not understood. Metamorphic core complexes are extensional structures that expose deep crust. As the understanding of MCC formation became clear in the 1980's, the adjacent Priest River MCC was identified and more field studies were conducted in the area, which led to a better understanding of the interaction between the Purcell trench and Hope faults. In the history of early geological study of the area, Daly (1906) first identified and named the narrow topographic low the Purcell trench. Calkins (1909) identified and named the Hope fault and reported evidence of faulting in the Purcell trench, which became a basis of a long-standing interpretation that the Hope fault cross-cuts the Purcell trench. Daly (1912) suggested the possibility that the Purcell trench represented a full graben. Kirkham and Ellis (1926) identified an east dipping fault along the Purcell trench to the north of the Lake Pend Oreille, which is a segment of what is now known as the Purcell Trench fault. Anderson (1930) extended the east dipping fault identified by Kirkham and Ellis (1926) to the south. In the geologic map by Anderson, the extended fault was cross-cut and offset by the Hope fault. Figure 3a shows an interpretation by Harrison and Schmidt (1971) and Harrison and others (1972), a full graben-style Purcell Trench faults that are cross-cut and offset by the Hope fault and its splayed segments in a dextral sense. Until the 1970's, some researchers did not document any faults along the Purcell trench (e.g., Park and Cannon, 1943; Miller and Engels, 1975).

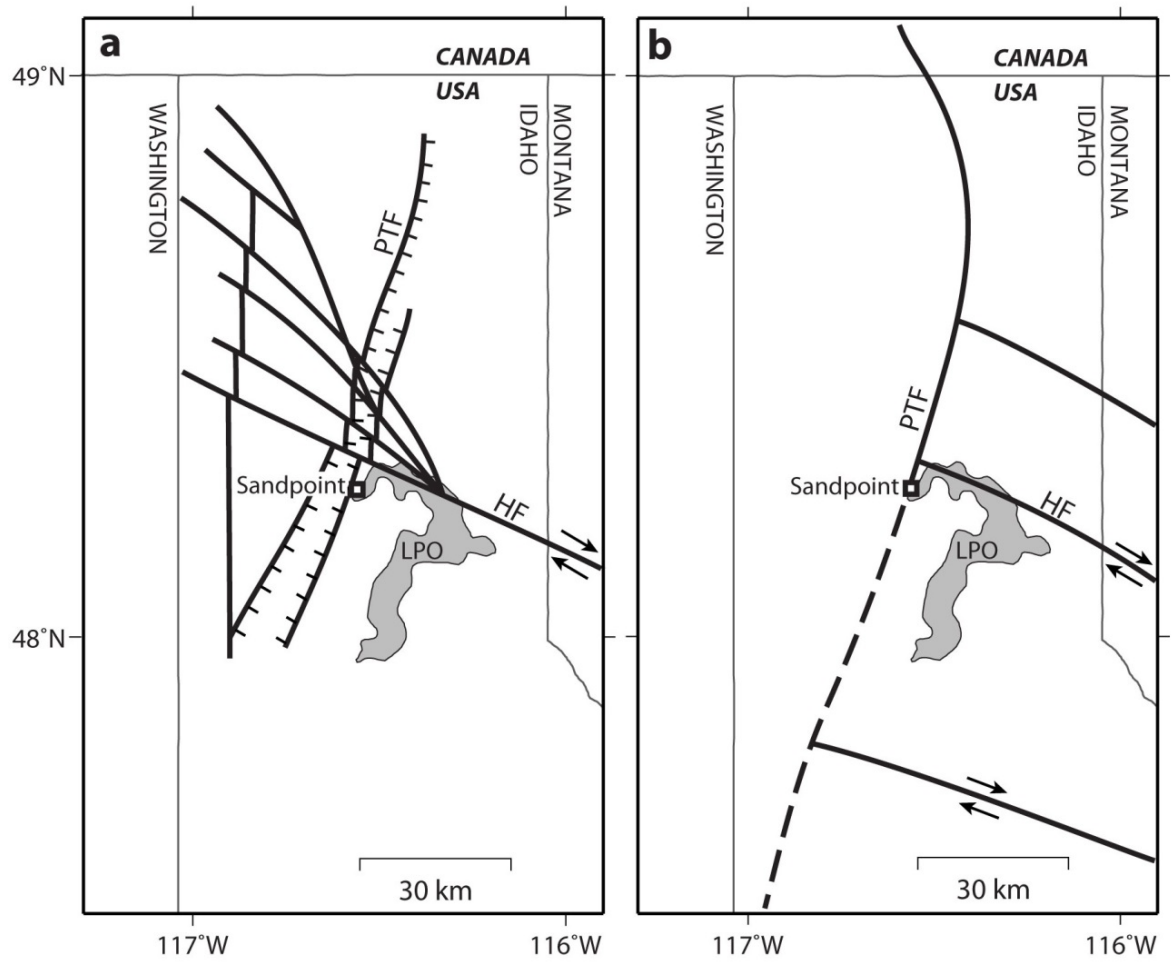

Figure 3**.** Simplified early interpretations of the relation between the Hope and Purcell Trench faults by (a) Harrison and others (1972) and (b) Clark (1973). PTF, Purcell Trench fault; HF, Hope fault; LPO, Lake Pend Oreille. Harrison and others (1972) show a full graben-style Purcell Trench faults that are cross-cut and offset by the Hope fault and its splayed segments. Clark (1973) shows the Hope fault system truncated against the Purcell Trench fault.

The current consensus about the relationship between the Hope and Purcell Trench faults is that: (1) the Purcell trench is a half-graben bounded on the west by the Purcell Trench fault; and (2) the Hope fault and its splayed segments are truncated against the east-southeast dipping Purcell Trench fault (Figure 2). These interpretations are also reflected in the geologic map by Bayley and Muehlberger (1968). Clark (1973) showed the dextral Hope fault system truncated against the Purcell Trench fault (Figure 3b). This interpretation has been adopted and refined by researchers who carried out field studies in the area (e.g., Harms, 1982; Harms and Price, 1992; Doughty and Price, 1999, 2000), and now widely accepted (e.g., Lewis and others, 2006, 2008; Foster and others, 2007).

The Newport fault system located to the west of the Purcell Trench fault and to the north of Newport, Washington, has a U-shaped trace with its opening in the north (Figure 2). The two fault tips are located ~15 km (~9 mi) south of the US-Canada border. The fault is shallowly dipping in a normal sense toward the center of the fault system (Rehrig and others, 1987; Harms and Price, 1992; Doughty and Price, 1999, 2000). The Newport fault delineates a partially isolated hanging-wall block underlain by the metamorphosed basement as a result of the formation of the Priest River MCC in response to Eocene extension (Figure 2) (Rehrig and others, 1987; Harms and Price, 1992; Doughty and Price, 1999, 2000).

The Packsaddle and Cascade faults traverse about 10-15 km (6-9 mi) southeast of the epicenters (Figure 2) (Lewis and others, 2008). They strike northeast-southwest and dip nearly vertically at the surface with the northwestern blocks structurally down dip. Their dip directions at greater depths are poorly known. If they formed in response to regional extension, these blocks should be dipping to the northwest. The faults formed during the Precambrian and were reactivated during the Cretaceous as a result of block tilting associated with a granodiorite intrusion, forming half-grabens (Harrison and Jobin, 1963; King and others, 1970).

The Lake Pend Oreille area has exhibited relatively low seismicity since regional seismic monitoring began in 1982. Figure 4 shows temporal distribution of seismicity in the area from 1988 through 2015 (see Appendix for the list of events). Detection and location of earthquakes prior to 1996, when northwestern Montana stations began operating, is probably reflective of an incomplete record for M<2.5 events. Small earthquakes have occurred annually in this area since 1999 except for a five-year period from 2004 to 2009. The first instrumentally located earthquake occurred about 15 km (9 mi) east-southeast of Sandpoint on June 18, 1988 with a magnitude of 3.4. Nine more earthquakes occurred from mid-1999 through mid-2003. The largest of these was a M3.5 event centered about 25 km (15.5 mi) south-southeast of Sandpoint on January 1, 2000. Ten additional small earthquakes occurred between 2009 and 2015, the largest was a magnitude 2.2 on August 3, 2014. The detection threshold appears to be about M1.5 since seismograph stations began operating in northwestern Montana in the late 1990’s. From this perspective, the 2015 seismicity exceeds any previous seismicity in the region since regional networks began operating (Figure 4b).

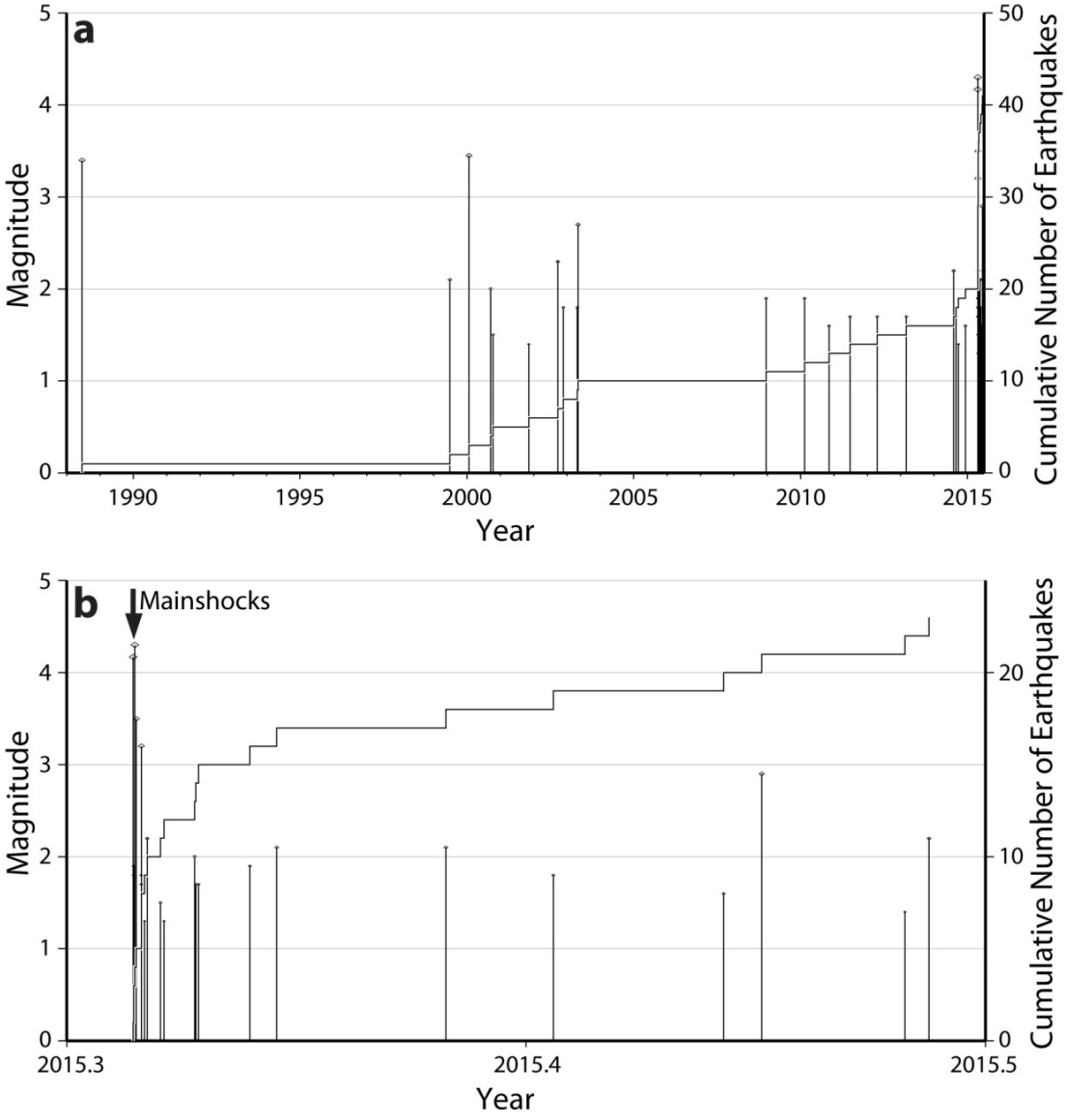

Figure 4**.** Timelines of instrumentally determined earthquakes in the Lake Pend Oreille area (lat 47.85° to 48.35°N. and long 116.00° to 116.75°W.; see Figure 2 for the area) (a) from 1988 through 2015, and (b) in 2015. Vertical bars topped by small diamonds (scaled to magnitude) indicate the date and magnitude of earthquakes (left scale). Stair-step curve indicates the cumulative number of earthquakes (right scale). Detection and location of earthquakes prior to 1996, when northwestern Montana stations began operating, is probably incomplete for M<2.5 events.

Figure 5 shows the spatial distribution of the instrumental earthquakes in the Lake Pend Oreille region since 1982. The largest earthquakes cluster within a three-kilometer diameter area at 48.10°N, 116.38°W, near the east shore of Lake Pend Oreille. Six events lie about 2.5 km (1.6 mi) northeast of the largest earthquakes and six small events (magnitudes 1.3 to 1.8) scatter up to 20 km (12 mi) northward. The north-south scatter of these epicenters very likely has more to do

with poor seismograph station distribution around the events (i.e., no station control north or south of the epicenters) than any sort of north-south trending seismogenic structure. This poor station geometry probably also contributes to the scattered distribution of smaller, pre-2015 earthquakes across the northeastern part of Lake Pend Oreille. A regional seismic network in northern Idaho would contribute to a better understanding of both tectonic and mining-related earthquakes in northern Idaho.

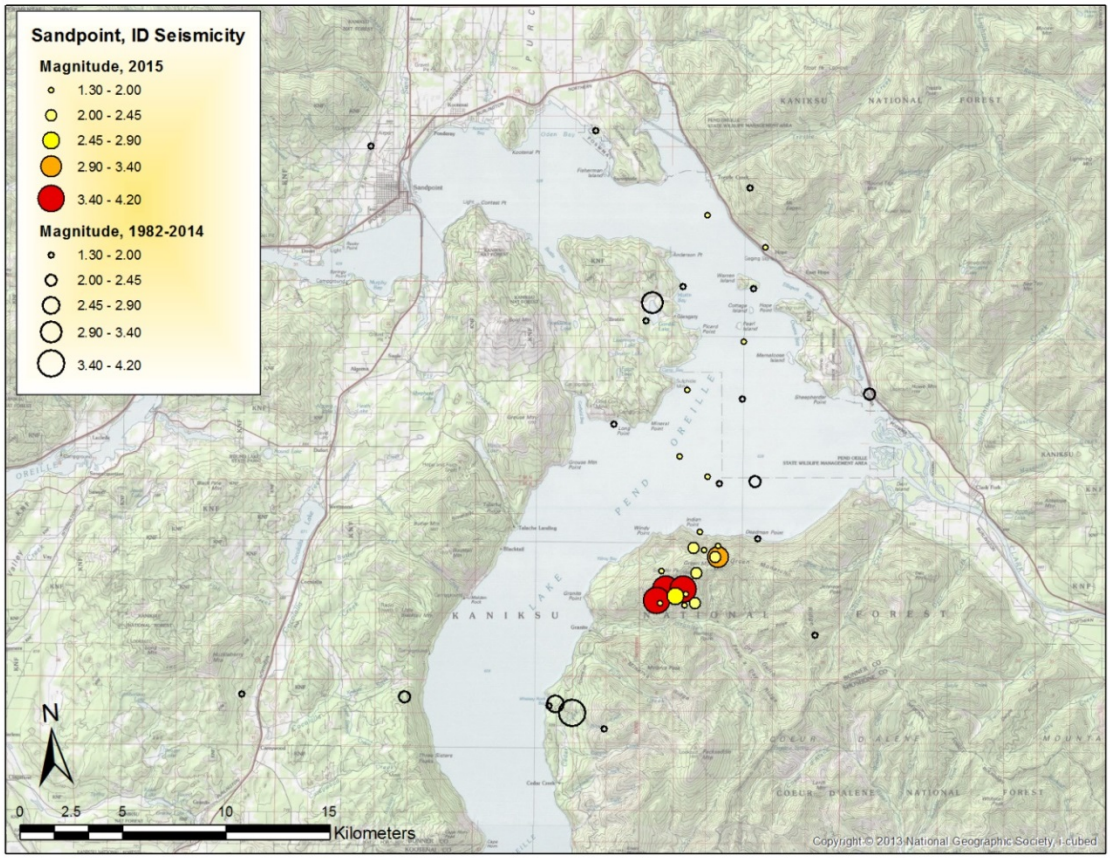

Figure 5. Spatial distribution of epicenters of events from 1982 through 2014 (open circles scaled by magnitude) and in 2015 (colored circles scaled by magnitude).

THE 24 APRIL 2015 SANDPOINT EARTHQUAKE SEQUENCE

The three principal events of the Sandpoint sequence occurred immediately southeast of Lake Pend Oreille within a radius of 2 km (1.2 mi) (Figure 6) at 02:32, 05:43, and 08:28 on April 24th, 2015 (UTC) (Table 1). Estimates of both hypocenter and origin time show good agreement between this study and the USGS for the size of the events (M~4). The largest discrepancy in hypocenter is of the first event and is ~3.9 km (~2.4 mi) (Table 1; Figure 6). The USGS (U.S. Geological Survey, 2015a) reports the horizontal uncertainty of the epicenter of the first event to be ±5.0 km (3.1 mil), whereas our estimation is ±1.2 km (0.7 mi). Therefore, the location

determined in this study is in the range of the uncertainty of the epicenter by the USGS. The second event has the largest magnitude (M4.2), and that of the first and third events are M4.1 and M3.5, respectively (Table 1). The earthquakes were felt in much of northeastern Washington and northern Idaho to northwestern Montana (U.S. Geological Survey, 2015a, b, c). Seismograms of the second event recorded at selected sites are shown in Figure 7.

The USGS estimated peak acceleration, peak velocity, and instrumental intensity (Worden and others, 2012) of the first and second events (Figure 8) (U.S. Geological Survey, 2015a, b). The first event made a record of peak acceleration at ~1.5 %g at ~10 km (6 mi) away from the epicenter, and at 0.3 %g at 30-40 km (19-25 mi) away from the epicenter (Figure 8a). The peak velocities are ~0.16 cm/s at 10 km (6 mi) away from the epicenter, and ~0.04 cm/s at ~ 30 km (19 mi) (Figure 8b). Weak shaking associated with intensity II-IV (Wood and Neumann, 1931; U.S. Geological Survey, 1989) was recorded in the radius of 50 km (31 mi) (Figure 8c). For the second event, at ~10 km (~6 mi) from the epicenter, the peak acceleration was 2.1 %g, and at ~50 km (~31 mi) 0.3 %g (Figure 8d). The peak velocity of ~0.18 cm/s and 0.03 cm/s were observed at ~10 km (~6 mi) and ~50 km (~31 mi), respectively, from the epicenter (Figure 8e). The second event caused weak shaking (intensity II-IV) in the radius of 60 km (37 mi) (Figure 8f). The second event was felt widely in northeastern Washington, northern Idaho, and northwestern Montana (U.S. Geological Survey, 2015b). For the Sandpoint area, the USGS (U.S. Geological Survey, 2014) estimates two- and ten-percent probabilities of exceeding 20%g and 7%g, respectively, in 50 years of peak ground acceleration. From the standpoint of the size of ground motion, the Sandpoint events were well predicted.

Small (M1-3) aftershocks have followed the Sandpoint earthquakes. They exhibit a typical temporal aftershock distribution for approximately two weeks following the mainshocks (Figure 4b). Six additional small earthquakes through the end of June, 2015 indicate a somewhat elevated rate of seismicity compared to 1999 to 2014 levels (Figure 4). Figure 5 shows the spatial distribution of the aftershocks (U.S. Geological Survey, 2015c). Most of the aftershocks are located south of the Hope fault and east of the Purcell Trench fault, and eight aftershocks are concentrated within a three-kilometer radius of the epicenters area of the main shocks (Figure 6).

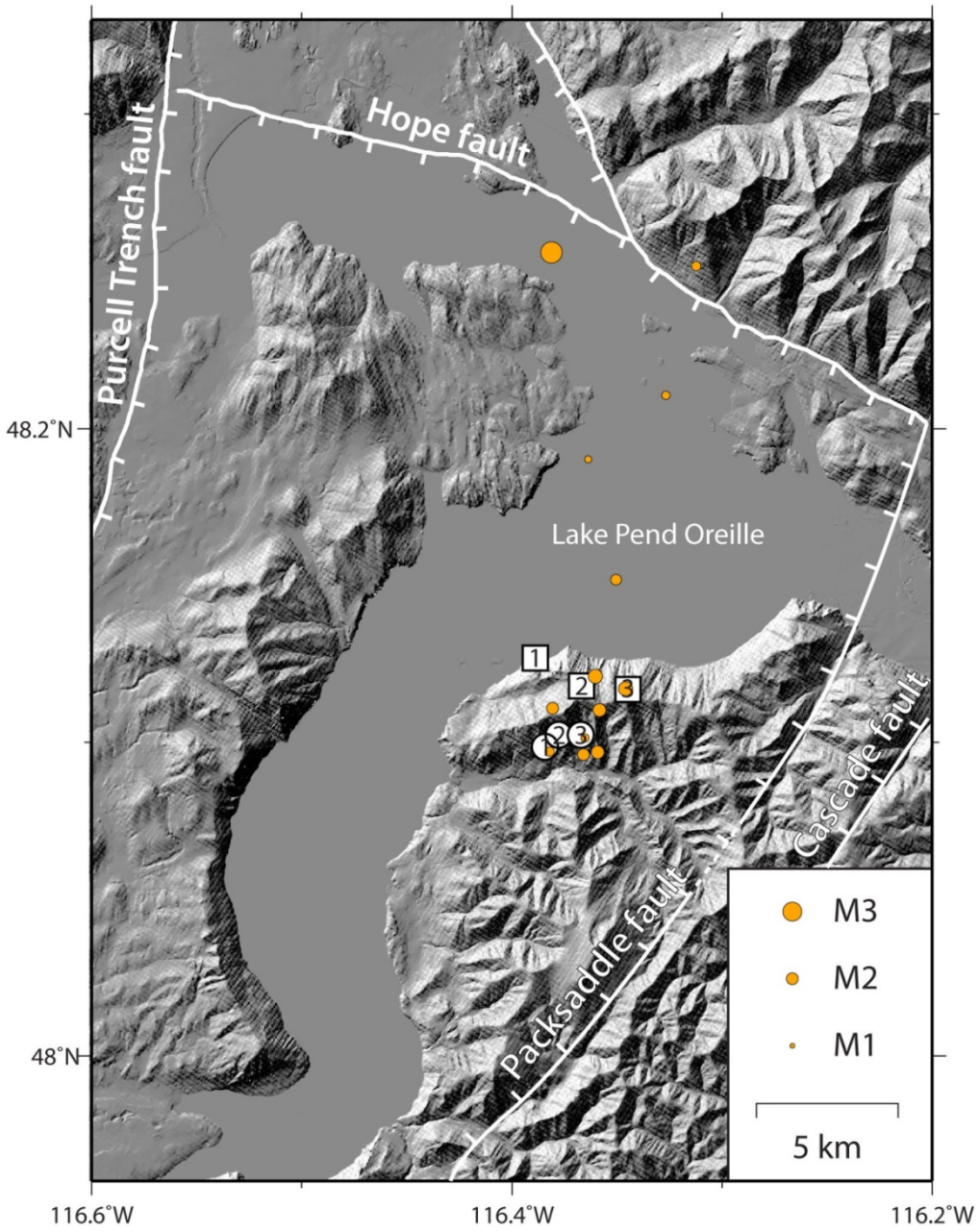

Figure 6**.** Epicenters of the Sandpoint earthquakes by this study (white circles) and the USGS (U.S. Geological Survey, 2015a, b; white squares), and aftershocks during the first three months after the Sandpoint events (orange dots). Number in symbol represents the order of an event in the Sandpoint sequence.

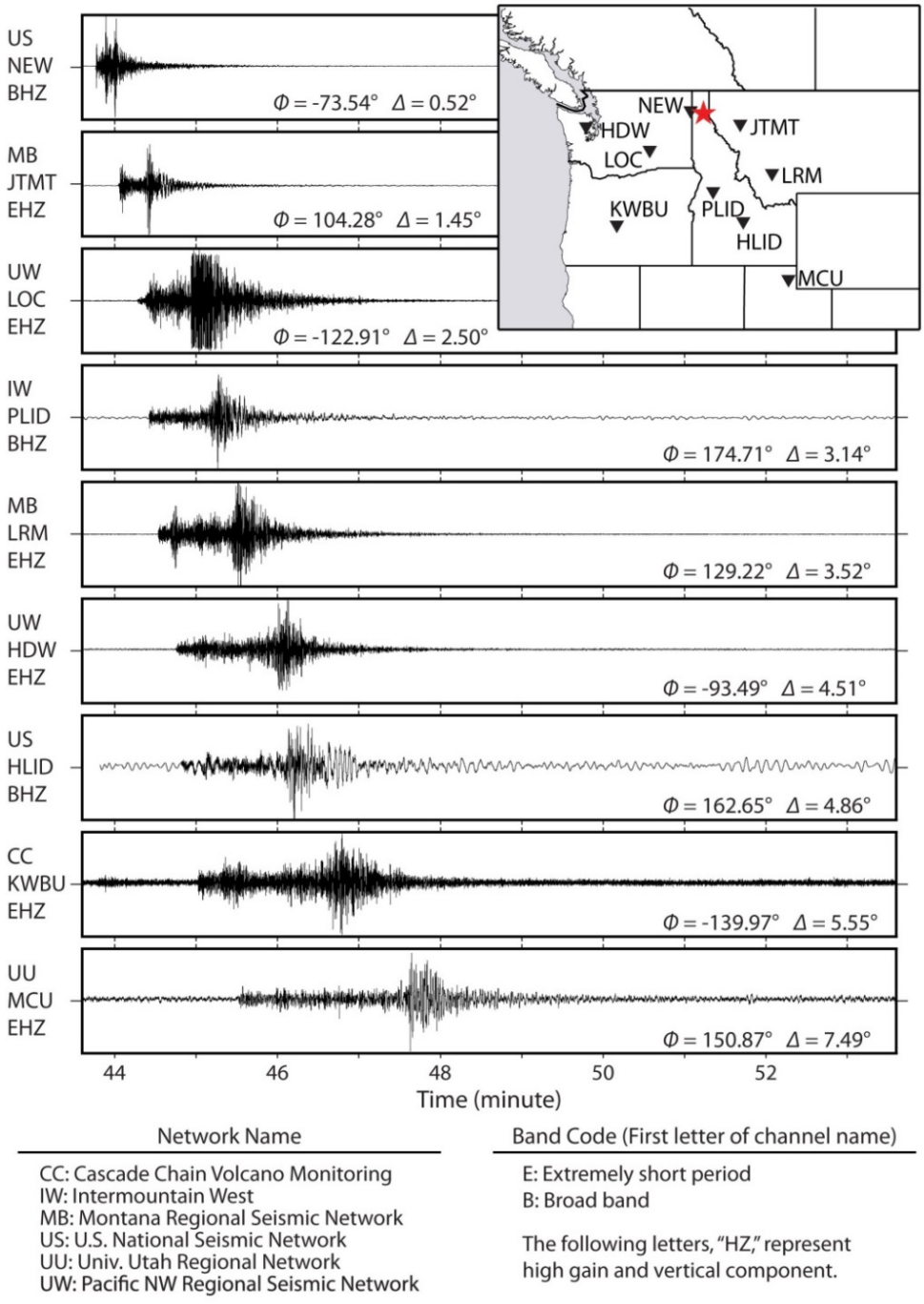

Figure 7. Seismograms of the second event of the Sandpoint sequence recorded at selected stations. All the seismograms are normalized vertical components. The origin of the time axis is the origin time of the second event at 05:43:36 (UTC). Network, station, and channel names are listed by the individual seismograms. Φ and Δ represent azimuth and distance, respectively. Inset shows the epicentral area (red star) and station locations (inverted triangles).

Table 1. Origin details of the Sandpoint earthquakes sequence on April 24th, 2015

	Event	Origin time (UTC)	Longitude	Latitude	Horizontal uncertainty (km)	Depth (km)	Vertical uncertainty (km)
This study	1	02:32 20.21	-116.384	48.099	± 1.2	14.0	± 1.1
	2	05:43 36.33	-116.378	48.103	± 1.3	14.2	± 1.3
	3	08:28 28.79	-116.367	48.103	± 1.2	11.7	± 1.1
USGS[a]	1	02:32 20.370	-116.389	48.127	± 5.0	11.5	± 2.9
	2[b]	05:43 36.400	-116.367	48.118	± 4.9	15.0	± 5.5
	3[b]	08:28 28.800	-116.345	48.117	± 4.4	9.5	± 6.3

	Event	Minimum Distance[c] (km)	Travel time residual (sec)	Azimuthal Gap (°)	Magnitude
This study	1	58.0	0.35	120	Md[d] 4.1
	2	58.0	0.37	120	Md 4.2
	3	59.0	0.34	121	Md 3.5
USGS[a]	1	56.77	0.64	36	M_{wr} 3.7
	2[b]	58.33	1.28	118	M_{wr} 3.9
	3[b]	59.89	1.00	118	M_l 3.3

[a] From U.S. Geological Survey (2015a, b)
[b] Location is determined by the Montana Bureau of Mines and Geology.
[c] Distance to the nearest station
[d] Coda duration magnitude (Eaton, 1992)

FAULT PLANE SOLUTIONS

We determined fault plane solutions for the three largest earthquakes using P-wave first motions from seismograph stations in Montana, Idaho, eastern Washington, and southern Canada. We used P-wave arrival times recorded at stations within 450 km (280 mi) of the epicenter and the western Montana crustal velocity model (Zeiler and others, 2005) together with HYPO71PC (Lee and Valdes, 1985) to determine earthquake hypocenters. The Newport, Washington, seismograph station (NEW; Figure 7) is the closest station to the epicenters at a distance of approximately 60 km (37 mi). The computed hypocenter depths range from about 10 to 14 km (6 to 9 mi) but are poorly constrained due to the lack of nearby seismograph stations. The fault plane solutions are presented in Table 2 and Figure 9 in lower hemisphere, equal-area projection. Moment tensor solutions of the first and second events reported by the USGS are also presented in Figure 10 for comparison.

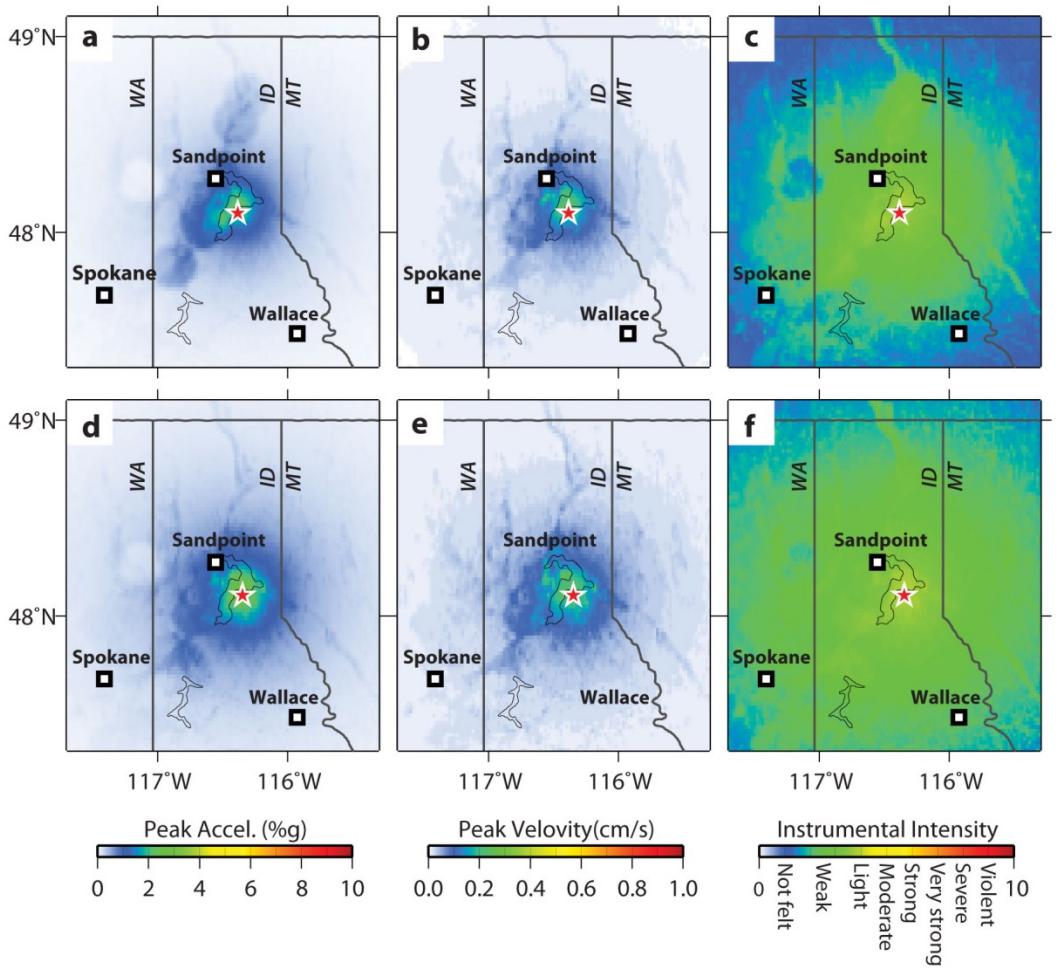

Figure 8**.** Recorded (a) peak acceleration, (b) peak velocity, and (c) instrumental intensity of the first event of the Sandpoint sequence, and (d-f) those of the second event. Data from the U.S. Geological Survey (2015a).

Table 2. Fault plane solution of the Sandpoint earthquakes

Event	Strike	Dip	Rake	Uncertainties (90% confidence range)			Number of first motion observations
				Strike	Dip	Rake	
1	42	28	66	8	8	15	54
2	50	35	80	18	5	20	43
3	80	50	100	3	0	10	22

The focal mechanism of the first event (Figure 9a; Table 2) indicates an oblique reverse motion with northeast striking nodal planes. The mechanism has a well-constrained southeast dipping nodal plane with a strike of 42 ± 8° and dip of 28 ± 8°. The other nodal plane strikes at 249° azimuth and dips at 65° to the north-northwest although this plane is not as well constrained as the first one. The tension axis is at a trend of 182° azimuth and a plunge of 68°, and the compressional axis at a trend of 330° azimuth and a plunge of 19°. Assuming the northeast striking plane represents the fault plane, the rake is 66° indicating a sinistral component. This lateral component is well constrained by stations located to the west-southwest of the hypocenter (i.e., DAVN, EPH, OD2, and WOLL; Figure 9a).

The fault plane solution of the second event is consistent with that of the first event (Figures 9b; Table 2). The northeast striking nodal plane strikes at 50° azimuth ± 18° and dips at 35 ± 5°SE. The other plane strikes at 242° azimuth and dips at 56°NW. The tension axis trends at 177° azimuth and plunges at 78°, and the compressional axis is at a trend of 327° azimuth and plunge of 10°. The second event also has a small lateral component; the rake on the northeast striking plane is 80°. This oblique slip is constrained by the reading of a station, DAVN (Figure 9b).

The third event also has a slightly oblique reverse mechanism consistent with the first event (Figure 9c; Table 2). The strike, dip, and rake of the northeast striking plane are 80° azimuth ± 3°, 50° ± 0°SE, and 100°, respectively. The other plane strikes at 245° azimuth and dips at 42° to the north-northwest. The tension axis orients at a trend of 43° azimuth and a plunge of 81°, and the compressional axis orients at a trend of 163° azimuth and a plunge of 5°.

Figure 10 and Table 3 present moment tensor solutions of the first two events reported by the USGS. The first event has a large discrepancy between our fault plane solution and the moment tensor solution by the USGS (2015a) (Figures 9a and 10a). The USGS' solution shows an oblique normal sense of motion with a north striking plane and an east-southeast striking plane (Figure 10a) (U.S. Geological Survey, 2015a) while our fault plane solution indicates a reverse motion with a northeast striking plane and west-southwest striking plane (Figure 9a). The USGS' moment tensor solution of the first event is also discrepant with that of the second event (Figure 10b) (U.S. Geological Survey, 2015b) although our P-wave first motion readings for both first and second events are very similar (Figures 9a and 9b). The comparisons make the moment tensor solution of the first event questionable. The large discrepancy may have resulted from the nature of the determination method of moment tensor solutions. Moment tensor solutions are obtained by analyzing low-frequency signals (i.e., period of tens to hundreds of seconds) of a waveform. If an earthquake is M~4 or smaller as in the case of the Sandpoint event, significant low frequency signals are not produced, which makes its moment tensor solution unreliable.

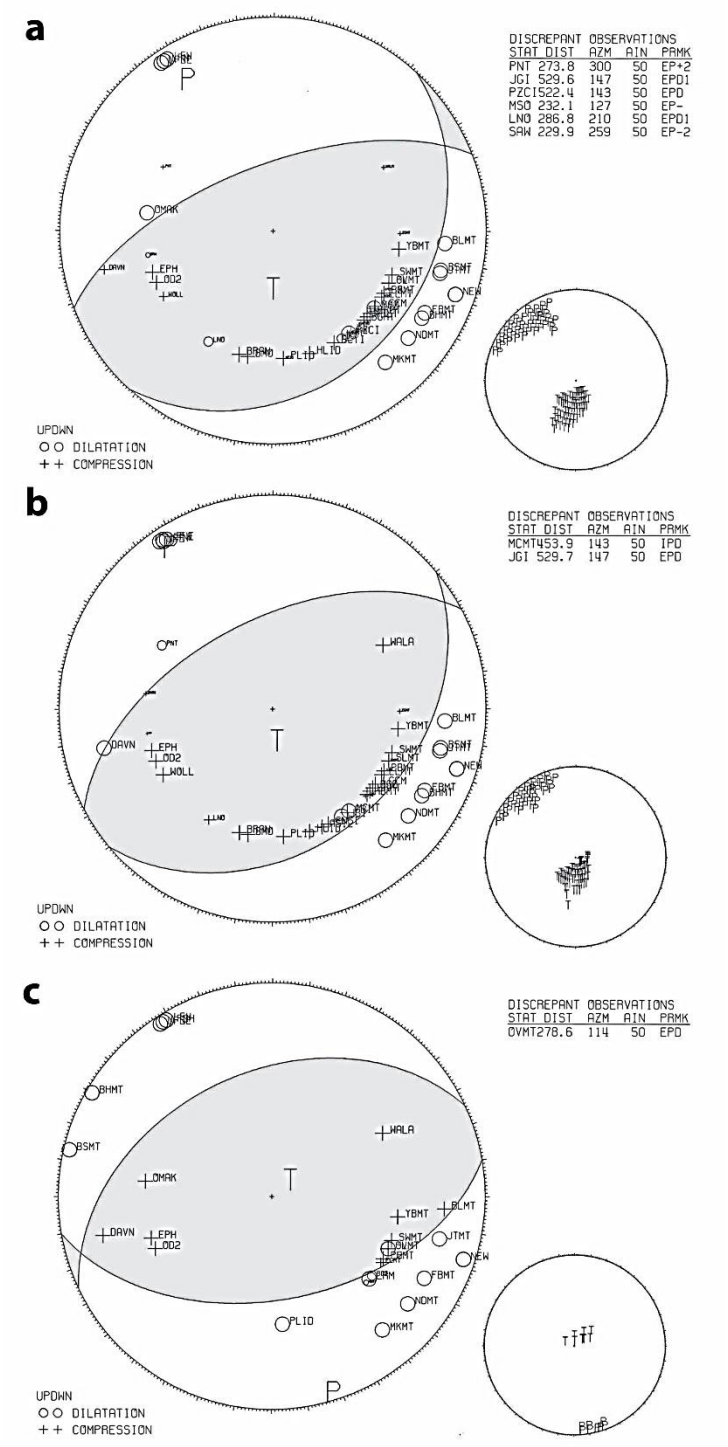

Figure 9**.** Fault plane solutions for the (a) first, (b) second, and (c) third events of the Sandpoint earthquakes. Symbols P and T mark the orientation of possible directions of the P and T axes, respectively, on an equal-area stereonet with lower hemisphere projection.

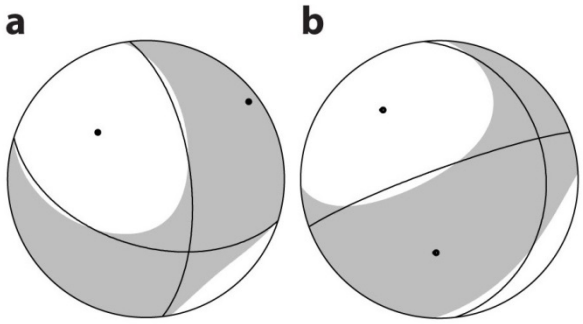

Figure 10. Moment tensor solutions for the (a) first and (b) second events of the Sandpoint earthquakes by the USGS (U.S. Geological Survey, 2015a, b). Dots mark the orientation of possible directions of the P and T axes. The moment tensor solution of the first event has a large discrepancy with the fault plane solution (Figure 7a).

Table 3**.** Source parameters of the Sandpoint earthquakes determined by the U.S. Geological Survey (2015a, b).

Event	Seismic moment ($\times 10^{14}$ Nm)	Magnitude	Depth (km)	Double Couple (%)	Strike	Dip	Rake
1	4.501	3.70	18.0	60	353	63	-45
2	7.597	3.85	20.0	37	251	84	113

Event	T axis			N axis			P axis		
	Value	Plunge	Azimuth	Value	Plunge	Azimuth	Value	Plunge	Azimuth
1	3.931	8	53	0.979	39	149	-4.910	50	314
2	5.868	46	184	2.714	23	68	-8.581	35	320

TECTONIC IMPLICATIONS

From the hypocenter locations of the earthquake sequence, it is probable that the events occurred either on the Hope fault or on the Purcell Trench fault (Figure 11a). None of the nodal planes of the sequence that generally strike northeast-southwest agree with the attitude of the southeast striking Hope fault. The well-defined nodal planes of the first and second events that strike at 42° and 50° azimuth respectively, are in agreement with the strike of the closest segments of the Purcell Trench fault (Figure 11a). The listric nature of the Purcell Trench fault (Reynolds, 1980; Rehrig and others, 1987; Doughty and Price, 1999, 2000) is also consistent with the shallow dip of the nodal planes at about 30°. Figure 11b shows a schematic cross section and the proposed mechanism of the first event, which is the best constrained, of the Sandpoint sequence with a rotated fault plane solution projected on the cross sectional plane. The

cross section is perpendicular to the surface trace of the closest segment of the Purcell Trench fault. The reverse mechanism on the Purcell Trench fault may represent a reactivation of the normal fault as a result of compression. Although the closest segment of the western termination of the Newport fault has a similar strike (10-30°) to the well-constrained nodal plane, its westerly dip does not agree with the nodal plane (Figure 11). Similarly, it is unlikely for the Packsaddle and Cascade faults to have slipped and cause the Sandpoint earthquakes as they dip to the northwest (Figure 11).

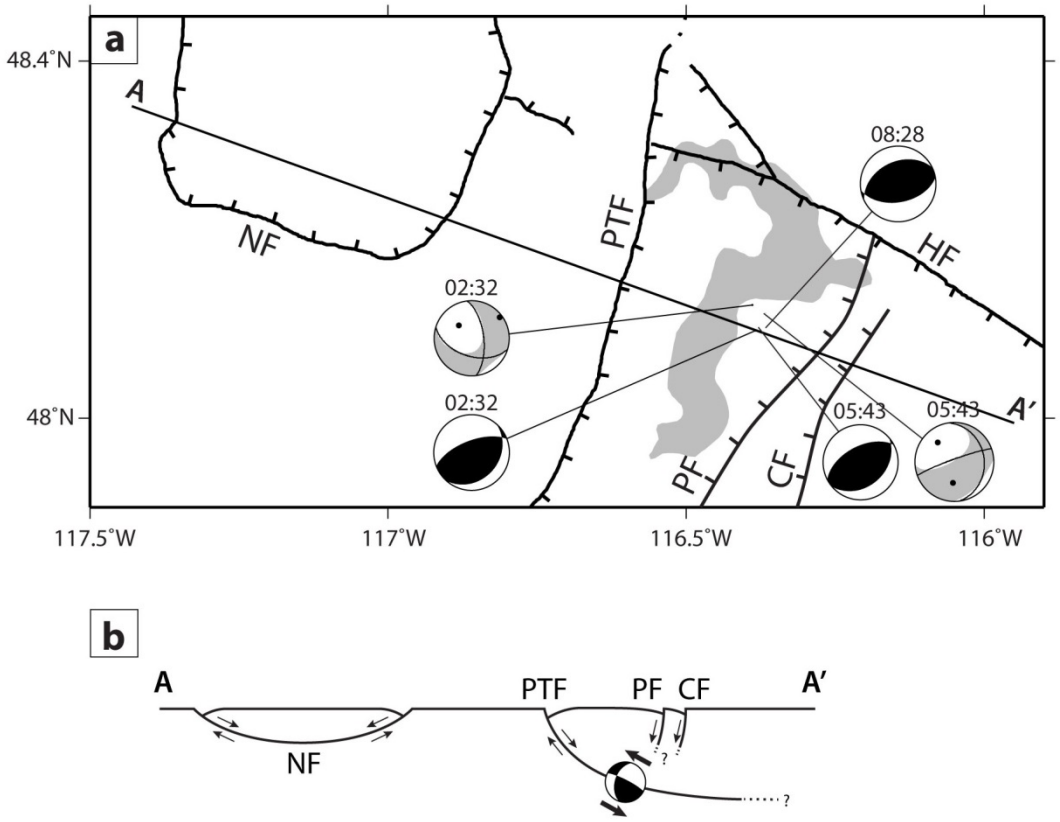

Figure 11. (a) Epicenters and focal mechanism solutions of the Sandpoint sequence by this study (black compressive quadrants) and the U.S. Geological Survey (2015a, b; gray compressive quadrants), and fault distribution in the epicentral area. Origin time is shown on each focal mechanism. NF, Newport fault; PTF, Purcell Trench fault; HF, Hope fault; PF, Packsaddle fault; CF, Cascade fault. Line A-A' indicates location of schematic cross section shown in Figure 9b. (b) Schematic cross section through the Newport and Purcell Trench Faults. The cross section is perpendicular to the surface trace of the Purcell Trench fault. Focal mechanism is for the fault plane solution of the first event of the Sandpoint sequence projected on the cross-sectional plane. The reverse mechanism (thick arrows) may represent a reactivation of the Purcell Trench fault.

It is tectonically reasonable to expect contractional deformation in the Sandpoint area. A recent GPS velocity field presented by McCaffrey and others (2013) in Figure 12 shows a large-scale clockwise crustal rotation in the northwestern United States relative to stable North America. The pole of rotation is in central Idaho. The trailing edge of the whole rotating region

is located around Yellowstone and the Wasatch Front in Utah, and the leading edge is diffuse in southeastern Washington. Kinematic block modeling by McCaffrey and others (2013) suggests that most compression around the leading edge is accommodated in the Yakima fold-thrust belt (YFTB) ranging from southeastern Washington to northeastern Oregon (Figure 12) (Reidel and others, 2003). It is possible that the residual compression is accommodated in a broader region including the epicentral area to the northeast of the YFTB (Figure 12).

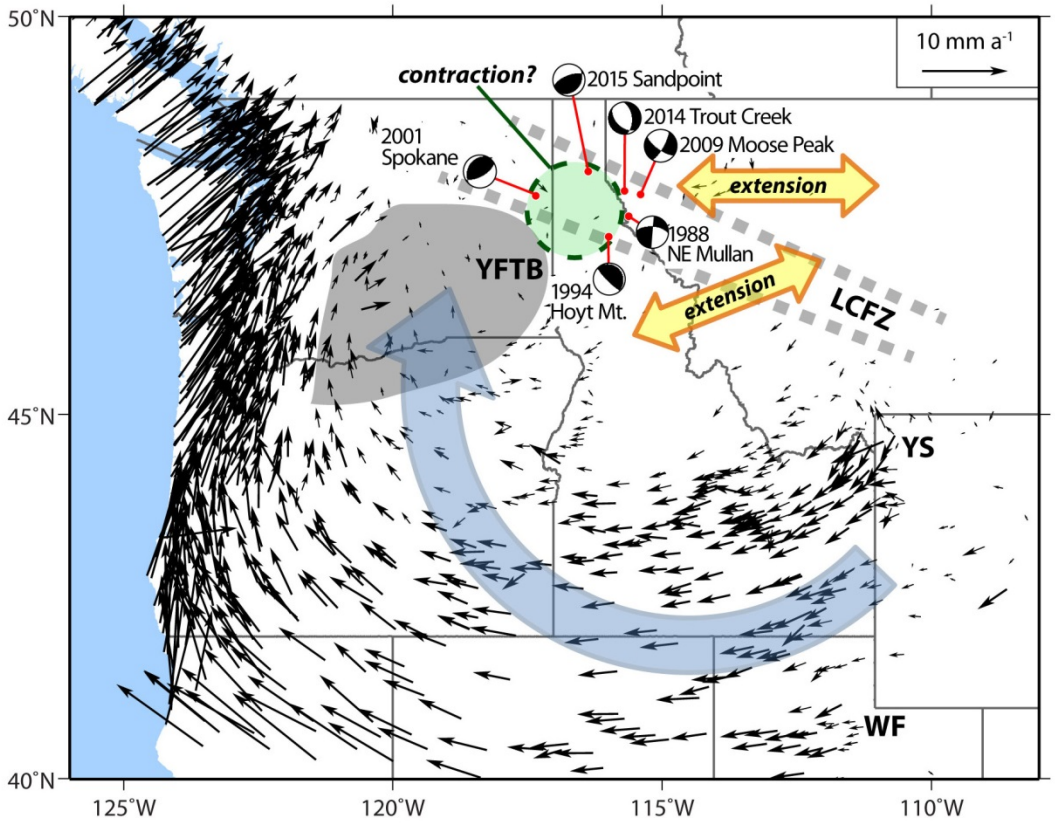

Figure 12. GPS velocity field of the northwestern U.S. (McCaffrey and others, 2007, 2013) showing a clockwise crustal rotation (blue arrow) relative to the North American plate. The leading edge of the rotating region is in the Yakima fold-thrust belt (YFTB; shaded area; Reidel and others, 2003), and the trailing edge is around Yellowstone (YS) and the Wasatch Front (WF). Extension directions indicated by seismicity (yellow arrows; Stickney, 2015). Dashed green circle indicates the area of possible contraction.

Past natural seismicity in the region indicates contractional deformation. The 1994 Hoyt Mountain earthquake, which occurred about 95 km (59 mi) south-southeast of the Sandpoint earthquakes, has a reverse mechanism on a northwest-southeast striking nodal plane (Figure 12) (Sprenke and others, 1994). The earthquake was followed by a M2.9 aftershock identical to the mainshock in location and focal mechanism (Sprenke and others, 1994). In 2001, a total of 105 shallow, small magnitude earthquakes occurred in the Spokane area (Wicks and others, 2013). The station distribution of the nearby seismic network was not optimal to determine the location

and mechanism of those small events. Wicks and others (2013) modeled a previously unknown blind fault and a collective slip direction indicated by the earthquake swarm, using InSAR data showing a pattern of surface deformation. The best fit model in the InSAR study suggests oblique thrusting on the fault that strikes northeast-southwest and dips at ~30° to the northwest (Wicks and others, 2013). The modeled fault plane and slip direction is shown in Figure 12 as a focal mechanism plot. Figure 13 shows T-axes of the Sandpoint earthquakes and the adjacent 2001 Spokane events. The T-axis plot indicates that the adjacent dextral slip events, the 1988 NE Mullan and 2014 Moose Peak events, are not kinematically compatible with the three earthquake sequences that indicate contractional deformation, the 1994 Hoyt Mountain, the 2001 Spokane, and the Sandpoint earthquakes (Figure 13). Therefore, the Sandpoint earthquakes, along with the Hoyt Mountain events and the Spokane swarm, constrain the western extent of the northeast-southwest extension of the LCFZ to the Idaho-Montana border area (Figures 12).

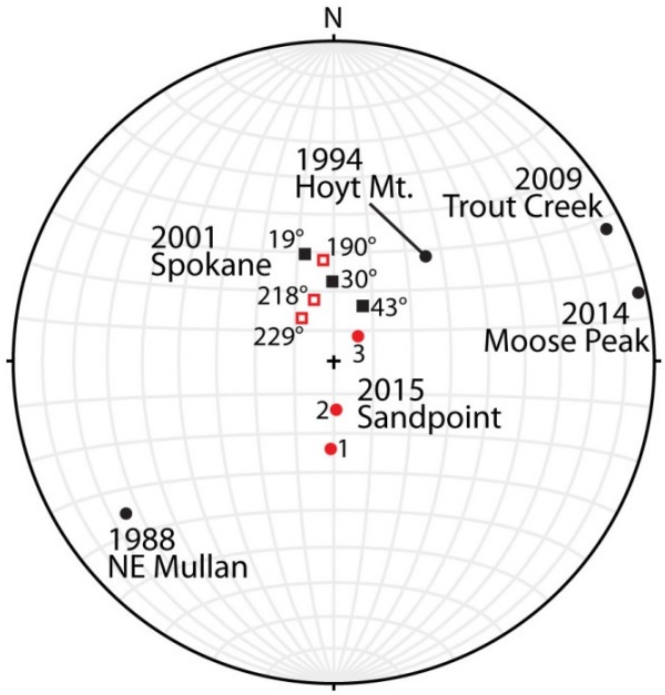

Figure 13. T-axes from fault plane solutions of the Sandpoint earthquakes (red dots) and the adjacent events (black dots; see Figure 12 for earthquake location), and from the best-fit (solid square) and alternate allowable (open square) models of the 2001 Spokane sequence (Wicks and others, 2013). Numbers by solid squares indicate a dip variation (minimum, best-fit, and maximum). Numbers by open squares indicate a strike variation (minimum, best-fit, and maximum) of the alternate allowable model. The dextral slip earthquakes, the 1988 NE Mullan and 2014 Moose Peak, and the normal-faulting 2009 Trout Creek event are not kinematically compatible with the three earthquake sequences that indicate contractional deformation.

It is also probable that the epicentral area is compressed by localized crustal deformation. Figure 14 shows a distribution of dilatational strain derived from the GPS horizontal velocities

(McCaffrey and others, 2007, 2013). If the velocity field is controlled mainly by localized crustal deformation, the Sandpoint area is compressed as indicated by weak contraction (i.e., negative dilatation of ~5-10 nanostrain/year) although it is poorly constrained (i.e., there is only one GPS site in the northeast part of the study area; Figure 13). Assuming that the slip of the Sandpoint events is in the order of meters, and that shortening rate in the area is in the order of millimeters per year, the order of the recurrence interval of the same type of earthquake on the same fault segment is thousands of years. The same type of earthquake, possibly M~5, can occur on a different segment of the Purcell Trench fault at any point in future; note that the 1942 M~5 event occurred in the Sandpoint area (Sprenke and Breckenridge, 1992) although its exact location is unknown. Since the general strike of the Purcell Trench fault is north-south (Figure 2), it is vital to have seismic stations in the Idaho Panhandle to determine what segment of the fault future earthquakes may occur on.

CONCLUSIONS

The largest first two events of the Sandpoint earthquake sequence on April 24th, 2015, have a focal mechanism indicative of an oblique reverse motion with a well-defined northeast striking nodal plane and a southwest striking nodal plane. The attitude of the well-constrained nodal plane well corresponds to the northeast striking, listric normal Purcell Trench fault. The events are likely to represent a reactivation of the Purcell Trench fault in a reverse sense as a result of regional compression. A regional velocity field and strain analysis suggests that the epicentral Sandpoint area is in a zone of weak contraction, which may be responsible for the reverse mechanism of the events. The 1994 Hoyt Mountain, the 2001 Spokane, and the 2015 Sandpoint earthquake sequences have reverse sense of motions and possibly mark the western extent of the northeast-southwest extension of the LCFZ. Seismic stations in northern Idaho would contribute to a better constraint on earthquake locations and enhance seismic predictions in the region.

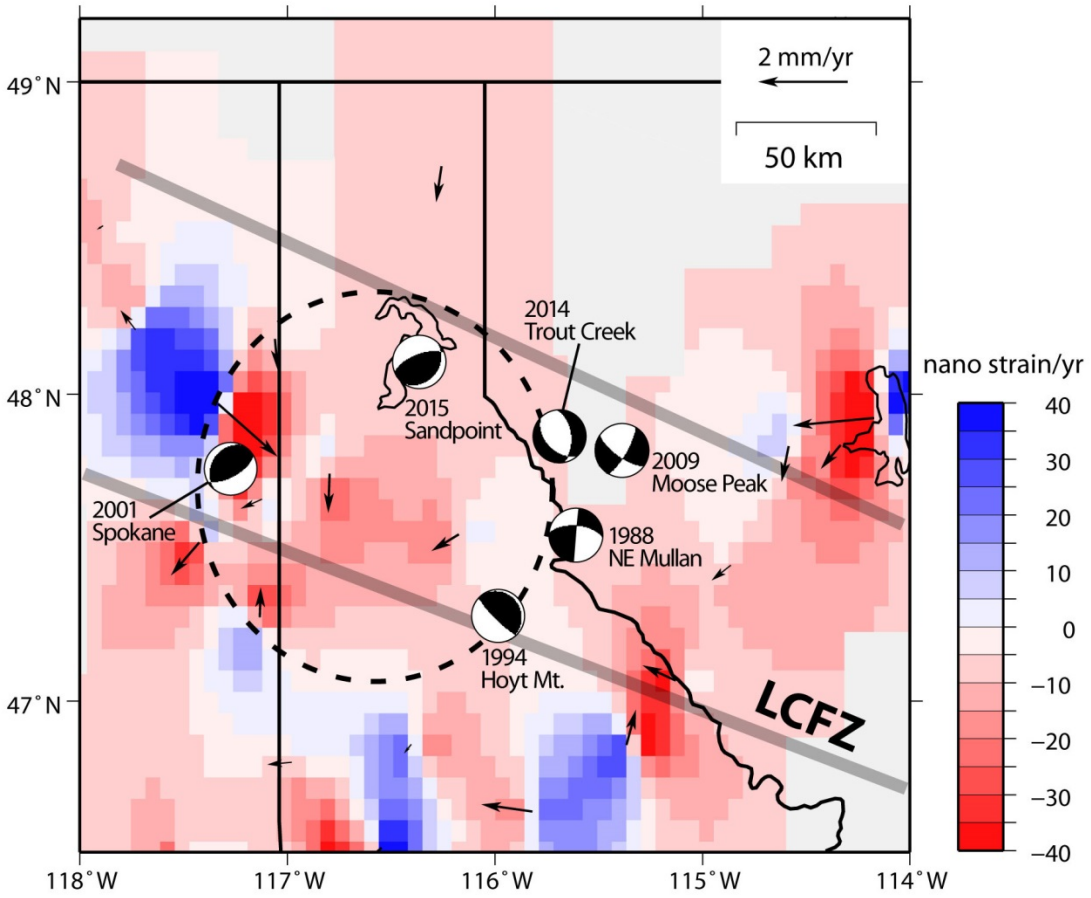

Figure 14**.** Dilatational strain rate (dilatation positive) calculated from GPS horizontal velocities. Thick gray lines bracket the LCFZ. Contractional strain (negative dilatation) is dominant in the proposed area of contraction (dashed circle) indicated by seismicity.

ACKNOWLEDGMENTS

We thank Russell Burmester and Reed Lewis for providing us with valuable comments on northern Idaho geology. Reed Lewis and Ed Ratchford reviewed the final manuscript. The use of seismic data recorded by the NIOSH Spokane Mining Research Division, the University of Washington, the University of Utah Seismograph Stations, the Idaho National Labs, the US Geological Survey, and the Canadian Geological Survey is gratefully acknowledged. The maps were produced using the Generic Mapping Tools (GMT) software, and the tension axes plot was produced using Stereonet 9.

REFERENCES

Anderson, A.L., 1930, Geology and ore deposits of the Clark Fork district, Idaho: Idaho Bureau of Mines and Geology Bulletin 12, 152p.

Bayley, R.W., and W.R. Muehlberger, 1968, Basement rock map of the United States (exclusive of Alaska and Hawaii): U.S. Geological Survey Map, scale 1:2,500,000.

Calkins, F.C., 1909, A geological reconnaissance in northern Idaho and northwestern Montana, with notes on the economic geology: U.S. Geological Survey Bulletin 384, 112p.

Clark, S.H.B., 1973, Interpretation of a high-grade Precambrian terrane in northern Idaho: Geological Society of America Bulletin, v. 84, p. 1999-2004.

Coney, P.J., 1987, The regional tectonic setting and possible causes of Cenozoic extension in the North American Cordillera *in* M.P. Coward, J.F. Dewey, and P.L. Hancock, eds., Continental Extensional Tectonics: Geological Society Special Publication 28, p. 177-186.

Daly, R.A., 1906, The nomenclature of the North American Cordillera between the 47th and 53d parallels of latitude: The Geographical Journal, v. 27, p. 586-606.

Daly, R.A., 1912, Geology of the North American Cordillera at the forty-ninth parallel: Canada Geological Survey Memoir 38, 546p.

Doughty, P.T., and S.D. Sheriff, 1992, Paleomagnetic evidence for en echelon crustal extension and crustal rotations in western Montana and Idaho: Tectonics, v. 11, p. 663-671.

Doughty, P.T., and R.A. Price, 1999, Tectonic evolution of the Priest River complex, northern Idaho and Washington: A reappraisal of the Newport fault with new insights on metamorphic core complex formation: Tectonics, v. 18, p. 375-393.

Doughty, P.T., and R.A. Price, 2000, Geology of the Purcell Trench rift valley and Sandpoint Conglomerate: Eocene en echelon normal faulting and synrift sedimentation along the eastern flank of the Priest River metamorphic complex, northern Idaho: Geological Society of America Bulletin, v. 112, p. 1356-1374.

Eaton, J.P., 1992, Determination of amplitude and duration magnitudes and site residuals from short-period seismographs in northern California: Bulletin of the Seismological Society of America, v. 82, p. 533-579.

Fillipone, J.A., and A. Yin, 1994, Age and regional tectonic implications of Late Cretaceous thrusting and Eocene extension, Cabinet Mountains, northwest Montana and northern Idaho: Geological Society of America Bulletin, v. 106, p. 1017-1032.

Fillipone, J.A., A. Yin, T.M. Harrison, G. Gehrels, M. Smith, and J.C. Sample, 1995, Age and magnitude of dip-slip faulting deduced from differential cooling histories: An example from the Hope fault, northwest Montana: The Journal of Geology, v. 103, p. 199-211.

Foster, D.A., and C.M. Fanning, 1997, Geochronology of the northern Idaho batholith and the Bitterroot metamorphic core complex: Magmatism preceding and contemporaneous with extension: Geological Society of America Bulletin, v. 109, p. 379-394.

Foster, D.A., P.T. Doughty, T.J. Kalakay, C.M. Fanning, S. Coyner, W.C. Grice, and J. Vogl, 2007, Kinematics and timing of exhumation of metamorphic core complexes along the Lewis and Clark fault zone, northern Rocky Mountains, USA *in* S.M. Roeske, A.B. Till, D.A. Foster, and J.C. Sample, eds., Exhumation Associated with Continental Strike-Slip Fault Systems: Geological Society of America Special Paper 434, p. 207-232.

Freidline, R.A., R.B. Smith, and D.D. Blackwell, 1976, Seismicity and contemporary tectonics of the Helena, Montana area: Bulletin of Seismological Society of America, v. 66, p. 81-95.

Gesch, D.B., 2007, The National Elevation Dataset, *in* D. Maune, eds., Digital Elevation Model Technologies and Applications: The DEM Users Manual, 2nd Edition: Bethesda, Maryland, American Society for Photogrammetry and Remote Sensing, p. 99-118.

Gesch, D., M. Oimoen, S. Greenlee, C. Nelson, M. Steuck, and D. Tyler, 2002, The National Elevation Dataset: Photogrammetric Engineering and Remote Sensing, v. 68, p. 5-11.

Harms, T.A., 1982, The Newport fault. Low-angle normal faulting and Eocene extension, northeast Washington and northwest Idaho: Queen's University M.S. thesis, 157 pp.

Harms, T.A., and R.A. Price, 1992, The Newport fault: Eocene listric normal faulting, mylonitization, and crustal extension in northeast Washington and northwest Idaho: Geological Society of America Bulletin, v. 104, p. 745-761.

Harrison, J.E., and D.A. Jobin, 1963, Geology of the Clark Fork quadrangle Idaho-Montana: U.S. Geological Survey Bulletin 1141-K.

Harrison, J.E., and P.W. Schmidt, 1971, Geologic map of the Elmira quadrangle, Bonner County, Idaho: U.S. Geological Survey Geological Quadrangle Map GQ-953, scale 1:63,500.

Harrison, J.E., M.D. Kleinkopf, and J.D. Obradovich, 1972, Tectonic events at the intersection between the Hope fault and the Purcell Trench, northern Idaho: U.S. Geological Survey Professional Paper, v. 719, 24p.

Harrison, J.E., A.B. Griggs, and J.D. Wells, 1974, Tectonic features of the Precambrian Belt basin and their influence on post-Belt structures: U.S. Geological Survey Professional Paper, v. 866, 15p.

Harry, D.L., D.S. Sawyer, and W.P. Leeman, 1993, The mechanics of continental extension in western north America: Implications for the magmatic and structural evolution of the Great Basin: Earth and Planetary Science Letters, v. 117, p. 59-71.

Hyndman, D.W., D. Alt, and J.W. Sears, 1988, Post-Archean metamorphic and tectonic evolution of western Montana and northern Idaho *in* W.G. Ernst, eds., Metamorphism and Crustal Evolution of the Western United States, Rubey Volume VII, p. 332-361.

King, E.R., J.E. Harrison, and A.B. Griggs, 1970, Geologic implications of aeromagnetic data in the Pend Oreille area, Idaho and Montana: U.S. Geological Survey Professional Paper, v. 646-D, 17p.

Kirkham, V.R.D., and E.W. Ellis, 1926, Geology and ore deposits of Boundary County, Idaho: Idaho Bureau of Mines and Geology Bulletin 10, 78p.

Lee, W.H.K., and C.M. Valdes, 1985, HYPO71PC: A personal computer version of the HYPO71 earthquake location program: U.S. Geological Survey Open-file Report 85-749, 44 p.

Lewis, R.S., R.F. Burmester, M.D. McFaddan, J.D. Kauffman, P.T. Doughty, W.L. Oakley, and T.P. Frost, 2005, Geologic map of the Headquarters 30 × 60 minute quadrangle, Idaho: Idaho Geological Survey Geologic Map, scale 1:100,000.

Lewis, R.S., R.F. Burmester, R.M. Breckenridge, S.E. Box, and M.D. McFaddan, 2006, Geologic map of the Sandpoint quadrangle, Bonner county, Idaho: Idaho Geological Survey Geologic Map, scale 1:24,000.

Lewis, R.S., R.F. Burmester, R.M. Breckenridge, M.D. McFaddan, and W.M. Phillips, 2008, Preliminary geologic map of the Sandpoint 30 x 60 minute quadrangle, Idaho and Montana, and the Idaho part of the Chewelah 30 x 60 minute quadrangle: Idaho Geological Survey Geologic Map, scale 1:100,000.

Livaccari, R.F., 1991, Role of crustal thickening and extensional collapse in the tectonic evolution of the Sevier-Laramide orogeny, western United States: Geology, v. 19, p. 1104-1107.

McCaffrey, R., A.I. Qamar, R.W. King, R. Wells, G. Khazaradze, C.A. Williams, C.W. Stevens, J.J. Vollick, and P.C. Zwick, 2007, Fault locking, block rotation and crustal deformation in the Pacific Northwest: Geophysical Journal International, v. 169, p. 1315–1340.

McCaffrey, R., R.W. King, S.J. Payne, and M. Lancaster, 2013, Active tectonics of northwestern U.S. inferred from GPS-derived surface velocities: Journal of Geophysical Research: Solid Earth, v. 118, p. 709-723.

Miller, F.K., and J.C. Engels, 1975, Distribution and trends of discordant ages of the plutonic rocks of northeastern Washington and northern Idaho: Geological Society of America Bulletin, v. 86, p. 517-528.

Northern California Earthquake Data Center, 2015, UC Berkeley Seismological Laboratory. Dataset. Available at: http://www.ncedc.org (accessed 1 August 2015).

Park, C.F., Jr., and R.S. Cannon Jr., 1943, Geology and ore deposits of the Metaline quadrangle, Washington: U.S. Geological Survey Professional Paper v. 202, 81 p.

Qamar, A.I., J. Kogan, and M.C. Stickney, 1982, Tectonics and recent seismicity near Flathead Lake, Montana: Bulletin of Seismological Society of America, v. 72, p. 1591-1599.

Rehrig, W.A., S.J. Reynolds, and R.L. Armstrong, 1987, A tectonic and geochronologic overview of the Priest River crystalline complex, northeastern Washington and northern Idaho in J.E. Schuster, eds., Selected Papers on the Geology of Washington: Washington Division of Geology and Earth Resources Bulletin 77, p. 1-14.

Reidel, S.P., B.S. Martin, H.L. Petcovic, 2003, The Columbia River flood basalts and the Yakima fold belt: Geological Society of America Field Guide 4, p. 87-105.

Reynolds, M.W., 1979, Character and extent of Basin-Range faulting, western Montana and east-central Idaho *in* G.W. Newman and H.D. Goode, eds., Basin and Range Symposium and Great Basin Field Conference: Denver, Colorado, Rocky Mountain Association of Geologists and Utah Geological Association, p. 185-193.

Reynolds, S.J., 1980, The Selkirk crystalline complex *in* P.J. Coney and S.J. Reynolds, eds., Cordilleran metamorphic core complexes and their uranium favorability: U.S. Department of Energy, p. 523-531.

Sbar, M.L., M. Barazangi, J. Dorman, C.H. Scholz, and R.B. Smith, 1972, Tectonics of the Intermountain Seismic Belt, western United States: Microearthquake seismicity and composite fault plane solutions: Geological Society of America Bulletin, v. 83, p. 13-28.

Sears, J.W., and W.J. Fritz, 1998, Cenozoic tilt domains in southwestern Montana: Interference among three generations of extensional fault systems *in* J.E. Faulds and J.H. Stewart, eds., Accommodation Zones and Transfer Zones: The Regional Segmentation of the Basin and Range Province: Geological Society of America Special Paper 323, p. 214-247.

Sears, J.W., M. Hendrix, A. Waddell, B. Webb, B. Nixon, T. King, E. Roberts, and R. Lerman, 2000, Structural and stratigraphic evolution of the Rocky Mountain foreland basin in central-western Montana *in* S. Roberts and D. Winston, eds., Geologic Field Trips, Western Montana and adjacent Areas: Rocky Mountain Section of the Geological Society of America, p. 131-155.

Sears, J.W., and M.S. Hendrix, 2004, Lewis and Clark line and the rotational origin of the Alberta and Helena salients, North American Cordillera *in* A.J. Sussman and A.B. Weil, eds., Orogenic Curvature: Integrating Paleomagnetic and Structural Analysis: Geological Society of America Special Paper 383, p. 173-186.

Smith, J.G., 1965, Fundamental transcurrent faulting in Northern Rocky Mountains: Bulletin of the American Association of Petroleum Geologists: v. 49, p. 1398-1409.

Sonder, L.J., P.C. England, B. Wernicke, and R.L. Christiansen, 1987, A physical model for Cenozoic extension of western North America *in* M.P. Coward, J.F. Dewey, and P.L. Hancock, eds., Continental Extensional Tectonics: Geological Society Special Publication 28, p. 187-201.

Sprenke, K.F., and R.M. Breckenridge, 1992, Seismic intensities in Idaho: Idaho Geological Survey Information Circular 50, 36p.

Sprenke, K.F., M.C. Stickney, D.A. Dodge, and W.R. Hammond, 1991, Seismicity and tectonic stress in the Coeur d'Alene mining district: Bulletin of the Seismological Society of America, v. 81, p. 1145-1156.

Sprenke, K.F., Stickney, M.C. and Breckenridge, R.M., 1994, The Hoyt Mountain earthquakes Shoshone County, Idaho March 7 and June 3, 1994: Idaho Geological Survey Staff Report 94-4, 20 p.

Stevenson, P.R., 1976, Microearthquakes at Flathead Lake, Montana: A study using automatic earthquake processing: Bulletin of Seismological Society of America, v. 66, p. 61-80.

Stickney, M.C., 1978, Seismicity and faulting of central western Montana: Northwest Geology, v. 7, 1-9.

Stickney, M.C., 1980, Seismicity and gravity studies of faulting in the Kalispell valley, northwestern Montana: University of Montana M.S. thesis, 82p.

Stickney, M.C., 2015, Seismicity within and adjacent to the eastern Lewis and Clark Line, west-central Montana: Northwest Geology, v. 44, p. 19-36.

Stickney, M.C., and M.J. Bartholomew, 1987, Seismicity and late Quaternary faulting of the northern Basin and Range Province, Montana and Idaho: Bulletin of the Seismological Society of America, v. 77, p. 1602-1625.

U.S. Geological Survey, 1989, The Severity of an Earthquake. U. S. Geological Survey General Interest Publication. U.S. Government Printing Office: 1989-288-913. Available at: http://pubs.usgs.gov/gip/earthq4/severitygip.html (accessed 25 August 2016).

U.S. Geological Survey, 2014, Seismic Hazard Lower 48 Maps and Data. Available at: http://earthquake.usgs.gov/hazards/products/conterminous (accessed 20 July 2015).

U.S. Geological Survey, 2015a, M3.7 – 20 km SW of Sandpoint, Idaho. Available at: http://earthquake.usgs.gov/earthquakes/eventpage/us200028q3#general_summary (accessed 1 June 2015).

U.S. Geological Survey, 2015b, M3.9 – 12 km ESE of Sandpoint, Idaho. Available at: http://earthquake.usgs.gov/earthquakes/eventpage/us200028ri#general_summary (accessed 1 June 2015).

U.S. Geological Survey, 2015c, M3.3 – 15 km ESE of Sandpoint, Idaho. Available at: http://earthquake.usgs.gov/earthquakes/eventpage/us200028sf#general_summary (accessed 1 June 2015).

Wallace, C.A., D.J. Lidke, and R.G. Schmidt, 1990, Faults of the central part of the Lewis and Clark line and fragmentation of the Late Cretaceous foreland basin in west-central Montana: Geological Society of America Bulletin, v. 102, p. 1021-1037.

Wernicke, B., R.L. Christiansen, P.C. England, and L.J. Sonder, 1987, Tectonomagmatic evolution of Cenozoic extension in the North American Cordillera, *in* M.P. Coward, J.F. Dewey, and P.L. Hancock, eds., Continental Extensional Tectonics: Geological Society Special Publication 28, p. 203-221.

Wicks, C., C. Weaver, P. Bodin, and B. Sherrod, 2013, InSAR evidence for an active shallow thrust fault beneath the city of Spokane Washington, USA: Journal of Geophysical Research: Solid Earth, v. 118, p. 1268-1276.

Winston, D., 1986, Middle Proterozoic tectonics of the Belt Basin, western Montana and northern Idaho *in* S.M. Roberts, eds., Belt Supergroup: A Guide to Proterozoic Rocks of Western Montana and Adjacent Areas: Montana Bureau of Mines and Geology Special Publication 94, p. 245-257.

Wood, H.O. and F. Neumann, 1931, Modified Mercalli intensity scale of 1931: Bulletin of the Seismological Society of America, v. 21, p. 277-283.

Worden, C.B., M.C. Gerstenberger, D.A. Rhoades, and D.J. Wald, 2012, Probabilistic relationships between ground-motion parameters and modified Mercalli intensity in California: Bulletin of the Seismological Society of America, v.102, p. 204-221.

Zeiler, C.P., M.C. Stickney, and M.A. Speece, 2005, Revised Velocity Structure of Western Montana: Bulletin of the Seismological Society of America, v. 95, p. 759-762.

APPENDIX

Earthquakes in the Lake Pend Oreille area (30 km in diameter centered at 48.175° N, 116.362 W°) from 1988 through 2015.

Year	Mo	Day	HrMn	Sec	Lat (N)	Lon (W)	Dep (km)	Mag	No[a]	Gap[b] (deg)	Dmin[c] (km)	RMS[d] (sec)	ErH[e] (km)	ErZ[f] (km)	Q[g]	Source	Location
1988	6	18	1444	13.7	48.228	116.387	5.0	3.4	24	-	-	-	-	-	-	NEIS[h]	15km E of Sandpoint, ID
2000	9	18	2249	19.3	48.303	116.424	0.6	2.0	10	332	131	0.23	4.3	4.3	D	MBMG[i]	10km NE of Sandpoint, ID
2000	10	11	1335	58.8	48.278	116.323	18.6	1.5	9	203	59.2	0.28	6.7	6.8	D	MBMG	15km E of Sandpoint, ID
2002	9	23	0838	50.5	48.188	116.245	11.6	2.3	15	185	65.5	0.29	4.5	3.8	D	MBMG	near Clark Fork, ID
2002	11	21	0622	46.8	48.235	116.367	6.7	1.8	10	196	56	0.37	10.8	9.3	D	MBMG	15km E of Sandpoint, ID
2003	4	23	1217	24.3	48.175	116.412	8.0	1.8	12	176	53.5	0.18	1.9	2	C	MBMG	15km SE of Sandpoint, ID
2010	11	8	1619	31.8	48.149	116.343	5.3	1.6	14	184	59.1	0.23	1.7	3.4	C	MBMG	13.3km W of Clark Fork, ID
2012	4	17	0125	43.4	48.220	116.391	27.9	1.7	9	193	54.3	0.11	3.5	1.2	D	MBMG	12.9km ESE of Sandpoint, ID
2013	3	2	0731	17.2	48.234	116.321	10.2	1.7	8	176	30.5	0.08	2.5	1.6	C	MBMG	1.8km SW of Hope, ID
2014	8	3	0612	35.7	48.150	116.320	5.0	2.2	17	138	60.8	0.37	2.3	2.7	D	MBMG	10.8km S of Hope, ID
2014	8	29	0654	55.5	48.125	116.318	15.9	1.7	10	135	61.5	0.14	1.7	2.7	C	MBMG	11.3km W of Clark Fork, ID
2014	9	21	0712	50.7	48.083	116.281	9.9	1.4	12	170	65.6	0.28	3.1	3.6	D	MBMG	10.2km WSW of Clark Fork, ID
2014	12	7	2211	47.1	48.186	116.328	17.4	1.6	9	189	59.5	0.32	7.9	7	D	MBMG	7km SSW of Hope, ID
2015	4	24	0232	20.3	48.118	116.370	14.3	4.4	36	121	58.1	0.3	1.5	1.7	D	MBMG	15.1km SSW of Hope, ID
2015	4	24	0246	50.5	48.122	116.344	8.2	1.9	14	135	59.8	0.26	2.4	2.6	C	MBMG	13.3km W of Clark Fork, ID
2015	4	24	0322	23.3	48.161	116.369	16.8	1.8	14	140	56.9	0.27	2.1	2.4	C	MBMG	10.7km SSW of Hope, ID
2015	4	24	0543	36.4	48.106	116.349	11.1	4.5	38	120	59.9	0.26	1	0.9	C	MBMG	13.9km WSW of Clark Fork, ID
2015	4	24	0828	28.8	48.117	116.345	9.6	3.6	32	121	59.9	0.22	1	1	C	MBMG	13.4km W of Clark Fork, ID
2015	4	24	1802	42.0	48.128	116.356	8.0	1.8	11	135	58.7	0.2	2.3	2.9	C	MBMG	13.7km SSW of Hope, ID
2015	4	24	1816	23.3	48.120	116.353	6.4	1.7	11	134	59.2	0.21	2.4	4.5	C	MBMG	14km W of Clark Fork, ID
2015	4	24	1839	10.7	48.117	116.344	7.8	3.2	20	134	59.9	0.2	1.4	1.3	C	MBMG	13.4km W of Clark Fork, ID
2015	4	24	2338	16.9	48.266	116.351	23.0	1.3	10	195	57.1	0.18	3.6	1.8	D	MBMG	4km WNW of Hope, ID
2015	4	25	0507	51.1	48.117	116.346	8.9	2.2	17	134	59.8	0.18	1.2	1.1	C	MBMG	13.5km W of Clark Fork, ID
2015	4	26	0650	12.2	48.101	116.365	6.6	1.5	8	175	59.0	0.22	3.1	7.3	D	MBMG	15.2km WSW of Clark Fork, ID
2015	4	26	1256	18.9	48.190	116.364	15.2	1.3	10	189	56.8	0.27	5.6	4.4	D	MBMG	7.6km SW of Hope, ID
2015	4	29	0034	41.7	48.096	116.366	5.7	2.0	12	165	59.1	0.27	3.1	4.8	D	MBMG	15.4km WSW of Clark Fork, ID
2015	4	29	0233	55.1	48.252	116.313	7.3	1.7	10	193	60.0	0.21	3.5	3	D	MBMG	0.7km NW of Hope, ID
2015	4	29	0730	11.4	48.097	116.382	6.1	1.7	10	170	57.9	0.26	3.4	6.3	D	MBMG	16.6km WSW of Clark Fork, ID
2015	5	3	0933	29.9	48.111	116.381	1.5	1.9	14	133	57.5	0.29	2.5	3.2	C	MBMG	16.1km W of Clark Fork, ID
2015	5	5	1311	20.5	48.110	116.358	7.1	2.1	14	172	59.1	0.16	1.6	1.5	C	MBMG	14.5km W of Clark Fork, ID
2015	5	19	0011	39.3	48.097	116.359	8.5	2.1	20	166	59.5	0.3	2.5	1.9	D	MBMG	14.9km WSW of Clark Fork, ID
2015	5	27	1332	33.2	48.152	116.351	4.0	1.8	12	178	58.5	0.21	2.3	3.6	C	MBMG	11.1km SSW of Hope, ID
2015	6	13	0416	28.2	48.100	116.372	14.5	2.9	26	120	58.5	0.34	1.8	2.1	D	MBMG	15.8km WSW of Clark Fork, ID

Earthquakes in the Lake Pend Oreille area (continued)

Year	Mo	Day	HrMn	Sec	Lat (N)	Lon (W)	Dep (km)	Mag	No[a]	Gap[b] (deg)	Dmin[c] (km)	RMS[d] (sec)	ErH[e] (km)	ErZ[f] (km)	Q[g]	Source	Location
2015	6	24	1318	37.1	48.211	116.327	6.4	1.4	9	187	59.2	0.15	2.4	4.6	C	MBMG	4.3km SSW of Hope, ID
2015	6	26	1121	41.7	48.121	116.360	2.8	2.2	13	134	58.6	0.28	2.1	4.1	C	MBMG	14.5km W of Clark Fork, ID

Data from Northern California Earthquake Data Center (2015).

[a] Number of P and S times

[b] Maximum azimuthal gap

[c] Distance to nearest station

[d] RMS travel time residual

[e] Horizontal error

[f] Vertical error

[g] Quality flag

[h] National Earthquake Information Service

[i] Montana Bureau of Mines and Geology